Constraints on Magnetic Braking from the G8 Dwarf Stars 61 UMa and τ Cet

Travis S. Metcalfe[1] , Klaus G. Strassmeier[2] , Ilya V. Ilyin[2] , Jennifer L. van Saders[3] , Thomas R. Ayres[4] ,
Adam J. Finley[5] , Oleg Kochukhov[6] , Pascal Petit[7] , Victor See[8] , Keivan G. Stassun[9] , Sandra V. Jeffers[10] ,
Stephen C. Marsden[11] , Julien Morin[12] , and Aline A. Vidotto[13]

[1] White Dwarf Research Corporation, 9020 Brumm Trail, Golden, CO 80403, USA; travis@wdrc.org
[2] Leibniz-Institut für Astrophysik Potsdam (AIP), An der Sternwarte 16, D-14482 Potsdam, Germany
[3] Institute for Astronomy, University of Hawaií, 2680 Woodlawn Drive, Honolulu, HI 96822, USA
[4] Center for Astrophysics and Space Astronomy, 389 UCB, University of Colorado, Boulder, CO 80309, USA
[5] Department of Astrophysics-AIM, University of Paris-Saclay and University of Paris, CEA, CNRS, Gif-sur-Yvette Cedex F-91191, France
[6] Department of Physics and Astronomy, Uppsala University, Box 516, SE-75120 Uppsala, Sweden
[7] Université de Toulouse, CNRS, CNES, 14 avenue Edouard Belin, F-31400, Toulouse, France
[8] European Space Agency (ESA), European Space Research and Technology Centre (ESTEC), Keplerlaan 1, 2201 AZ Noordwijk, The Netherlands
[9] Vanderbilt University, Department of Physics & Astronomy, 6301 Stevenson Center Lane, Nashville, TN 37235, USA
[10] Max-Planck-Institut für Sonnensystemforschung, Justus-von-Liebig-weg 3, D-37077, Göttingen, Germany
[11] Centre for Astrophysics, University of Southern Queensland, Toowoomba, Queensland, 4350, Australia
[12] Centre national de la recherche scientifique (CNRS), Université de Montpellier, Place Eugène Bataillon, F-34095, Montpellier, France
[13] Leiden Observatory, Leiden University, PO Box 9513, 2300 RA, Leiden, The Netherlands

Abstract

During the first half of their main-sequence lifetimes, stars rapidly lose angular momentum to their magnetized winds, a process known as magnetic braking. Recent observations suggest a substantial decrease in the magnetic braking efficiency when stars reach a critical value of the Rossby number, the stellar rotation period normalized by the convective overturn timescale. Cooler stars have deeper convection zones with longer overturn times, reaching this critical Rossby number at slower rotation rates. The nature and timing of the transition to weakened magnetic braking have previously been constrained by several solar analogs and two slightly hotter stars. In this Letter, we derive the first direct constraints from stars cooler than the Sun. We present new spectropolarimetry of the old G8 dwarf τ Cet from the Large Binocular Telescope, and we reanalyze a published Zeeman Doppler image of the younger G8 star 61 UMa, yielding the large-scale magnetic field strengths and morphologies. We estimate mass-loss rates using archival X-ray observations and inferences from Lyα measurements, and we adopt other stellar properties from asteroseismology and spectral energy distribution fitting. The resulting calculations of the wind braking torque demonstrate that the rate of angular momentum loss drops by a factor of 300 between the ages of these two stars (1.4–9 Gyr), well above theoretical expectations. We summarize the available data to help constrain the value of the critical Rossby number, and we identify a new signature of the long-period detection edge in recent measurements from the Kepler mission.

Unified Astronomy Thesaurus concepts: Spectropolarimetry (1973); Stellar evolution (1599); Stellar magnetic fields (1610); Stellar rotation (1629); Stellar winds (1636)

1. Introduction

Seven years after the suggestion that weakened magnetic braking (WMB) might explain the anomalously rapid rotation of old Kepler field stars (van Saders et al. 2016), the debate has shifted from whether this transition actually occurs to the specific physical mechanisms that might drive it. Although the original sample included just 21 stars, the analysis was subsequently extended (van Saders et al. 2019) to reproduce the properties of 34,000 Kepler field stars with measured rotation periods (McQuillan et al. 2014). The truncated distribution of rotation periods that led to the WMB hypothesis has now been confirmed using a sample of 94 stars with rotation rates measured from asteroseismology (Hall et al. 2021), and the predicted overdensity of stars with a range of ages near the long-period edge of the distribution has been confirmed (David et al. 2022) using more than 10,000 stars

with precise effective temperatures from LAMOST spectra (Xiang et al. 2019).

Evidence quickly surfaced that the interruption to stellar rotational evolution was probably caused by an underlying transition in stellar magnetism. The influence of magnetic morphology on the rate of angular momentum loss from stellar winds (Garraffo et al. 2015; Réville et al. 2015) led to the initial suggestion that WMB could be driven by a shift from a simple dipole to higher-order fields (van Saders et al. 2016). Preliminary support for this interpretation was identified (Metcalfe et al. 2016) in measurements of the large-scale magnetic field strength and morphology from Zeeman Doppler imaging (Petit et al. 2008) and was reinforced by the associated changes in stellar activity cycles (Metcalfe & van Saders 2017). Targeted observations for an evolutionary sequence of two stars slightly hotter than the Sun (Metcalfe et al. 2019, 2021), followed by a sequence of several solar analogs (Metcalfe et al. 2022), provided the first direct evidence of a magnetic morphology shift in older solar-type stars and placed new constraints on the relative importance of various contributions to the overall reduction in the wind braking torque. Such

constraints may ultimately help to identify a corresponding transition in the stellar dynamo.

In this Letter, we present the first direct constraints on the nature and timing of WMB from stars that are cooler than the Sun. In Section 2, we describe spectropolarimetric observations for an evolutionary sequence of two G8 dwarf stars, and we adopt other stellar properties largely from published sources. In Section 3, we use the prescription of Finley & Matt (2018) to estimate the wind braking torque for each star, confirming a dramatic decrease in the rate of angular momentum loss as seen previously for solar analogs and slightly hotter stars. Finally, we summarize the available constraints, and we identify a new signature of the long-period detection edge in recent measurements from the Kepler mission.

2. Observations

2.1. Spectropolarimetry

We observed τ Cet on 2022 September 18 from the 2×8.4 m Large Binocular Telescope (LBT) using the Potsdam Echelle Polarimetric and Spectroscopic Instrument (Strassmeier et al. 2015). The instrumental setup and data reduction methods were identical to those described in Metcalfe et al. (2019), and we employed the least-squares deconvolution (LSD) technique (Kochukhov et al. 2010) to derive precise mean intensity and polarization profiles. We obtained the line data required for the LSD analysis from the VALD database (Ryabchikova et al. 2015), adopting stellar atmospheric parameters from Brewer et al. (2016) and $v \sin i = 0.4$ km s^{-1} from Saar & Osten (1997). Because τ Cet has a 50 yr record of constant chromospheric activity (Baum et al. 2022) and appears to have a nearly pole-on orientation that minimizes rotational modulation (Gray & Baliunas 1994), we assume that our snapshot observation is representative of the mean stellar activity level. The value of $\log R'_{HK}$ for τ Cet is above recent solar minimum levels (Egeland et al. 2017) although the actual value may be slightly lower due to its subsolar metallicity (Saar & Testa 2012). There is no observational evidence to suggest that the low activity level of τ Cet represents a magnetic grand minimum; it appears similar to other constant-activity stars like ρ CrB and 16 Cyg A & B.

By combining the information from 1463 metal lines deeper than 5% of the continuum, we obtained a mean Stokes V profile with an uncertainty of 5.8 ppm (see Figure 1). The data yielded a statistically marginal detection of the circular polarization signature for τ Cet, with a mean longitudinal magnetic field $\langle B_z \rangle = -0.37 \pm 0.08$ G. Following Metcalfe et al. (2019) we modeled the line profile assuming an axisymmetric dipole magnetic field with the inclination fixed at $i = 20°$ (see Section 2.2), yielding a formal best fit $B_d = -0.77 \pm 0.31$ G. Note that the derived magnetic field strength does not depend strongly on the inclination (e.g., $B_d = -0.73$ G for $i = 5°$).

To complement the new LBT observations with another star along an evolutionary sequence, we reanalyzed a Zeeman Doppler imaging (ZDI) map for the younger G8 star 61 UMa (See et al. 2019), which was obtained near the minimum of its 4 yr activity cycle. This ZDI map was based on 21 Stokes V measurements obtained in 2008 with the NARVAL spectropolarimeter on the 2.03 m Télescope Bernard Lyot. Folsom et al. (2018) provide details of the ZDI inversion procedure, while Jardine et al. (2013) discuss the connection between the resulting magnetic fields at the surface and in the corona. The
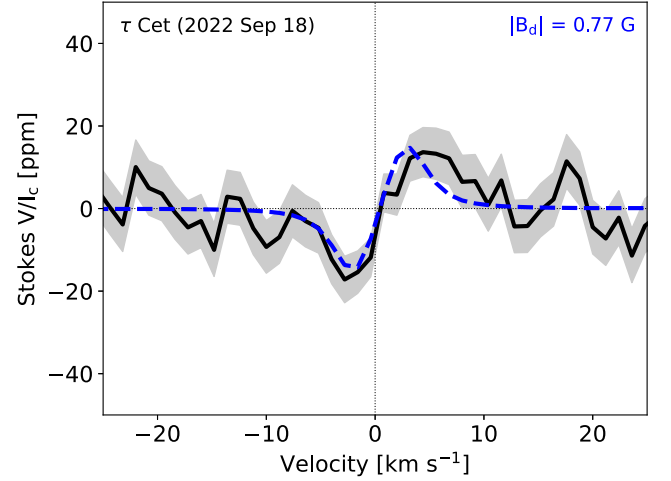

Figure 1. Stokes V polarization profile for τ Cet from LBT observations on 2022 September 18. The mean profile is shown as a black line with uncertainties indicated by the gray shaded area. The dashed blue line is an axisymmetric model profile assuming dipole morphology with the inclination fixed at $i = 20°$.

Table 1
Stellar Properties of 61 UMa and τ Cet

	61 UMa	τ Cet	Sources
T_{eff} (K)	5502 ± 78	5333 ± 78	1
[M/H] (dex)	-0.07 ± 0.07	-0.44 ± 0.07	1
$\log g$ (dex)	4.52 ± 0.08	4.60 ± 0.08	1
$B - V$ (mag)	0.72	0.72	2
$\log R'_{HK}$ (dex)	-4.546	-4.958	2
P_{rot} (days)	17	34	2
$|B_d|$ (G)	11.5	0.77	3
$|B_q|$ (G)	12.0	...	3
$|B_o|$ (G)	6.12	...	3
L_X (10^{27} erg s^{-1})	26.9 ± 0.6	0.49 ± 0.10	4
Mass-loss rate ($\dot{M}_\odot$)	9.6 ± 0.6	<0.1	4, 5
Mass ($M_\odot$)	0.94 ± 0.06	0.783 ± 0.012	4, 6
Radius ($R_\odot$)	0.845 ± 0.015	0.816 ± 0.012	4, 7
Luminosity ($L_\odot$)	0.588 ± 0.007	0.473 ± 0.011	4
Age (Gyr)	1.4 ± 0.2	9.0 ± 1.0	8, 9
Torque (10^{30} erg)	7.7	<0.026	10

References. (1) Brewer et al. (2016), (2) Baliunas et al. (1996), (3) Section 2.1, (4) Section 2.2, (5) Wood (2018), (6) Teixeira et al. (2009), (7) von Braun & Boyajian (2017), (8) Barnes (2007), (9) Tang & Gai (2011), (10) Section 3.

wind braking prescription of Finley & Matt (2018) requires the polar strengths of axisymmetric dipole, quadrupole, and octupole magnetic fields (B_d, B_q, B_o) as input, but the observed ZDI map contains both axisymmetric and nonaxisymmetric components. We followed the procedure described in Metcalfe et al. (2022) to calculate the equivalent polar field strengths for use with the wind braking prescription. This procedure captures the radial dependence of the magnetic flux for all components of the field, which is what matters for angular momentum loss. The results of this analysis for 61 UMa are shown in Table 1. There may be slight inconsistencies between the observed ZDI map and the equivalent polar field strengths derived in this way, but Jardine et al. (2013) demonstrated that the differences arise from nonradial components of the field, which induce near-surface magnetic stresses without altering the source

surface of the stellar wind. Consequently, they are unimportant for our estimation of the wind braking torque.

2.2. Stellar Properties

In addition to the magnetic field strength and morphology, the wind braking prescription of Finley & Matt (2018) also depends on the mass-loss rate ($\dot{M}$), the rotation period ($P_{\rm rot}$), and the stellar radius and mass (R, M). For τ Cet we adopted the upper limit on the mass-loss rate from Wood (2018), which was obtained directly from Lyα measurements. The rotation period was determined from time series observations of chromospheric activity by Baliunas et al. (1996), while the radius was inferred from interferometry (von Braun & Boyajian 2017) and the mass was adopted from asteroseismology (Teixeira et al. 2009). The stellar age was derived from an analysis of these same asteroseismic observations by Tang & Gai (2011). Our estimate of the inclination $i = 20°$ in Section 2.1 was calculated from the values of $v \sin i$, $P_{\rm rot}$, and R.

For 61 UMa, we determined the X-ray luminosity (L_X) from the ROSAT All-Sky Bright Source Catalog (Boller et al. 2016), following the approach described in Ayres & Buzasi (2022). When combined with the radius inferred from the spectral energy distribution (SED), following the procedures described in Stassun et al. (2017, 2018), this led to an X-ray flux per unit surface area that could be used to estimate the mass-loss rate from the empirical relation $\dot{M} \propto F_X^{0.77}$ (Wood et al. 2021). The rotation period of 61 UMa was determined from chromospheric activity measurements (Baliunas et al. 1996), while the mass was estimated from the SED radius using the empirical mass–radius relation from eclipsing binaries (Torres et al. 2010). The age of 61 UMa was determined from the gyrochronology relation of Barnes (2007), which remains valid for younger stars.

3. Wind Braking Torque

We now have all of the observational inputs that are required to estimate the wind braking torque using the prescription of Finley & Matt (2018).[14] For 61 UMa we have the equivalent polar field strengths ($B_{\rm d}$, $B_{\rm q}$, $B_{\rm o}$) from our reanalysis of the published ZDI map. For τ Cet we have the snapshot observation from LBT, which we model with an axisymmetric dipole field inclined at $i = 20°$ (below, in this Section, we assess the influence of adopting a different inclination or morphology). We estimate the mass-loss rate ($\dot{M}$) from the X-ray flux for 61 UMa, but we infer it directly from Lyα measurements for τ Cet (below we assess the influence of the higher mass-loss rate estimated from the X-ray flux for τ Cet). The remaining parameters ($P_{\rm rot}$, R, M) do not produce substantial uncertainties in the torque. Using the parameter values listed in Table 1 for our fiducial models, we find that the wind braking torque decreases by a factor of 300 between the ages of 61 UMa and τ Cet (1.4–9 Gyr).

By changing the wind braking prescription one parameter at a time between the values for 61 UMa and τ Cet, we can evaluate the relative importance of various contributions to the overall decrease in the torque. We find almost equal contributions from the evolutionary change in mass-loss rate (−92%) and the difference in magnetic field strength and morphology (−91%), with smaller contributions from the

---
[14] https://github.com/travismetcalfe/FinleyMatt2018

evolutionary change in rotation period (−50%) and differences in the stellar radius (−10%) and mass (+4%). Rotational evolution models use the Rossby number (Ro) to scale the mass-loss rate as $\dot{M} \sim {\rm Ro}^{-2}$ and the magnetic field strength as $B \sim P_{\rm phot}^{0.5}/{\rm Ro}$, where $P_{\rm phot}$ is the photospheric pressure (van Saders & Pinsonneault 2013), but they do not directly account for changes in magnetic morphology. Considering either WMB or standard spin down, these models predict a decrease in the wind braking torque of less than a factor of 15, with a smaller contribution from the evolutionary change in the mass-loss rate (−70% to −82%) and a difference from the change in magnetic field strength (−40% to −52%) that suggests a substantial contribution from a shift in magnetic morphology.

The large decrease in wind braking torque between the ages of 61 UMa and τ Cet is robust against changes to our assumptions about the magnetic field and mass-loss rate. For example, τ Cet has a debris disk with a measured inclination ($i = 35° \pm 10°$; Lawler et al. 2014). If we assume that the rotation axis of τ Cet shares this same inclination, the inferred dipole field would be slightly stronger ($B_{\rm d} = -0.89$ G) and produce a corresponding increase in the wind braking torque (0.029×10^{30} erg, +14%). If we keep $i = 20°$ but model the Stokes V profile as an axisymmetric quadrupole or octupole field, enhanced geometric cancellation would lead us to infer a stronger field ($B_{\rm q} = -2.94$ G or $B_{\rm o} = -118.9$ G). For a quadrupole field, this ultimately leads to a lower wind braking torque (0.023×10^{30} erg; −11%) because the stronger field does not compensate for the shorter effective lever arm. By contrast, the much stronger octupole field would ultimately produce a higher torque (0.043×10^{30} erg, +67%) despite the much shorter effective lever arm although this scenario is incompatible with the measured chromospheric activity level. Finally, if we use the X-ray flux of τ Cet to estimate its mass-loss rate ($0.46 \dot{M}_\odot$) following the same approach as for 61 UMa, the wind braking torque would more than double (0.058×10^{30} erg, +129%). However, even if we adopt both the octupole field and the higher mass-loss rate for τ Cet (contradicting the actual measurements of $\log R'_{\rm HK}$ and $\dot{M}$ shown in Table 1), the wind braking torque would still be 50 times weaker than for 61 UMa.

We can assess the empirical value of the critical Rossby number (Ro$_{\rm crit}$) by plotting the available estimates of wind braking torque on a common scale. We use the asteroseismic calibration of Corsaro et al. (2021) for the convective overturn timescale to calculate Ro for each star in our sample based on the Gaia $G_{\rm BP} - G_{\rm RP}$ color. The results are shown in Figure 2 with points grouped by Gaia color, corresponding to solar analogs (yellow circles) and hotter (blue triangles) or cooler stars (red squares). Our empirical constraint on the critical value of Ro on this scale (Ro$_{\rm crit} = 0.457 \pm 0.006$) is shown with a vertical dashed line. Our new estimates of the wind braking torque for 61 UMa and τ Cet extend the range of Ro sampled by our spectropolarimetric targets and show the highest and lowest torques of the ensemble. By construction, the more active stars in our sample (61 UMa, 88 Leo, HD 76151) are all below Ro$_{\rm crit}$, while the less active stars (16 Cyg A & B, ρ CrB, 18 Sco, τ Cet) are all above it. The Rossby numbers of HD 76151 (Ro = 0.451) and 16 Cyg A (Ro = 0.463) currently define the empirical constraint on the value of Ro$_{\rm crit}$ shown above, falling slightly below the solar value (Ro$_\odot = 0.496$) where we plot the solar wind braking torque determined by Finley et al. (2018).
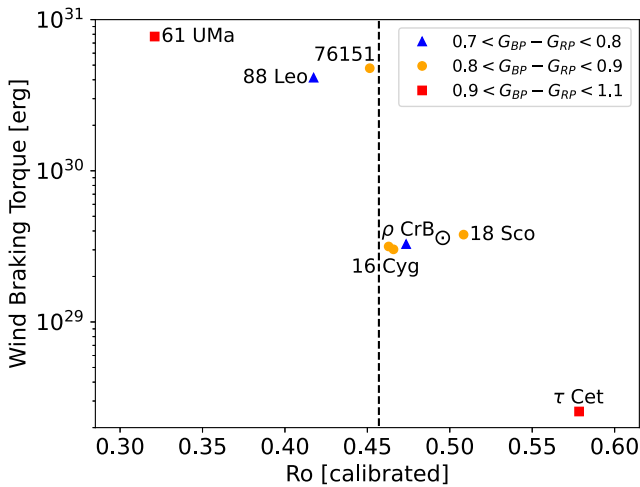
Figure 2. Evolution of the wind braking torque with Ro from the calibration of Corsaro et al. (2021). Points are grouped by Gaia color, corresponding to solar analogs (yellow circles) and hotter (blue triangles) or cooler stars (red squares). The empirical constraint for Ro_{crit} on this scale is shown with a vertical dashed line.

Figure 3. Rotation−activity relation for stars published in Corsaro et al. (2021), with the critical value of Ro from Section 3 shown as a vertical dashed line. Bright asteroseismic targets are shown with red circles. The highest density of stars (yellow and green) exhibit a broad range of activity levels at nearly constant Ro, which may correspond to the long-period edge of the Kepler sample.

4. Discussion

Using spectropolarimetric constraints on the large-scale magnetic field, we have demonstrated that the rate of angular momentum loss due to stellar winds decreases by a factor of 300 between the ages of two stars that are cooler than the Sun, dominated by contributions from both the mass-loss rate and the magnetic field strength and morphology. Relative to previous comparisons for solar analogs and slightly hotter stars, there is a larger evolutionary gap between 61 UMa and τ Cet, which would naturally lead to a more substantial decrease in the strength of magnetic braking across Ro $_{crit}$. On the other hand, the estimated wind braking torque for τ Cet could be even smaller because the mass-loss rate from Wood (2018) is an upper limit. For the solar analogs 16 Cyg A & B, Metcalfe et al. (2022) estimated a factor of 15–16 decrease in the wind braking torque relative to HD 76151, while for the slightly hotter star ρ CrB, Metcalfe et al. (2021) estimated a factor of 13 decrease relative to 88 Leo. However, these estimates all adopted upper limits on the magnetic field strengths from statistical nondetections of the Stokes V signatures, so the actual decreases could be larger. Our marginal detection of the Stokes V signature for τ Cet was facilitated by lower noise levels and by the nearly pole-on orientation, which minimizes geometric cancellation for an axisymmetric dipole magnetic field.

From a sample of 40,000 Kepler targets with measured rotation periods, Corsaro et al. (2021) plotted a photometric proxy for stellar activity (S_{ph}; Mathur et al. 2014) against the newly calibrated values of Ro (see Figure 3). Despite the vertical dispersion at all values of Ro due to activity cycles and inclination effects, the highest density of stars in their sample (yellow and green) appears at Ro slightly below the solar value, showing a broad range of stellar activity levels (Santos et al. 2019, 2021) at nearly constant Ro. This feature may correspond to the long-period edge of the Kepler sample (McQuillan et al. 2014; van Saders et al. 2019), where stellar activity gradually declines with age at roughly constant rotation period during the second half of main-sequence lifetimes (Metcalfe et al. 2016; Metcalfe & van Saders 2017). However, the relatively uniform distribution of bright asteroseismic targets (red circles) across
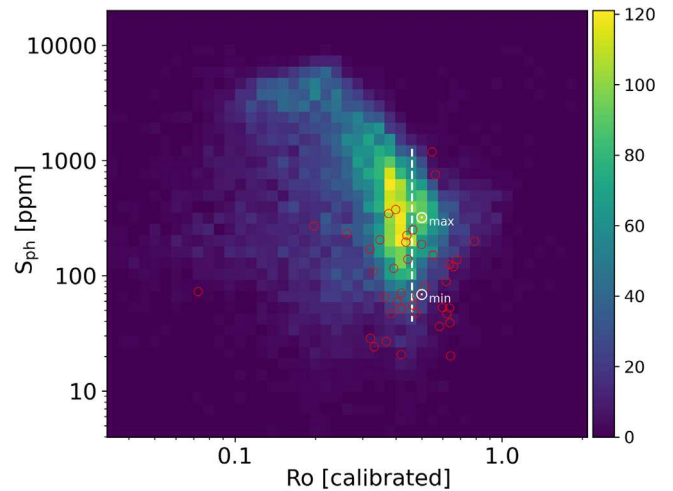
our empirical value of Ro_{crit} and toward low values of S_{ph} suggests that the detection of rotational modulation may simply be less efficient at higher Ro and lower S_{ph} (van Saders et al. 2019; Masuda 2022).

Future spectropolarimetry promises to extend our measurements to even cooler K-type stars and provide additional constraints on the empirical value of Ro_{crit}. Snapshot observations at LBT are already planned for HD 103095 and HD 166620. Although HD 103095 is an early K-type star, its extremely low metallicity ([M/H] = −1.16; Valenti & Fischer 2005) gives it the shallower convection zone of a late G-type star similar to τ Cet. With an activity cycle of 7.3 yr and a measured rotation period of 31 days (Baliunas et al. 1995, 1996), it will sample intermediate conditions (Ro = 0.542) between 61 UMa and τ Cet and probe how the driving mechanisms of WMB change over time. Observations of HD 166620 will complement our existing measurements of the active star 40 Eri, probing the magnetic morphology of a K-type star that recently entered a grand magnetic minimum (Baum et al. 2022; Luhn et al. 2022). Archival ZDI maps of younger K-type stars like ϵ Eri (Jeffers et al. 2014) and 61 Cyg A (Boro Saikia et al. 2016) from the BCool collaboration will provide additional context for our understanding of how magnetic braking shapes the lives of other Sun-like stars.

ORCID iDs

Travis S. Metcalfe ⓘ https://orcid.org/0000-0003-4034-0416
Klaus G. Strassmeier ⓘ https://orcid.org/0000-0002-6192-6494
Ilya V. Ilyin ⓘ https://orcid.org/0000-0002-0551-046X
Jennifer L. van Saders ⓘ https://orcid.org/0000-0002-4284-8638
Thomas R. Ayres ⓘ https://orcid.org/0000-0002-1242-5124
Adam J. Finley ⓘ https://orcid.org/0000-0002-3020-9409
Oleg Kochukhov ⓘ https://orcid.org/0000-0003-3061-4591
Pascal Petit ⓘ https://orcid.org/0000-0001-7624-9222
Victor See ⓘ https://orcid.org/0000-0001-5986-3423
Keivan G. Stassun ⓘ https://orcid.org/0000-0002-3481-9052
Sandra V. Jeffers ⓘ https://orcid.org/0000-0003-2490-4779
Stephen C. Marsden ⓘ https://orcid.org/0000-0001-5522-8887
Julien Morin ⓘ https://orcid.org/0000-0002-4996-6901
Aline A. Vidotto ⓘ https://orcid.org/0000-0001-5371-2675

References

Ayres, T., & Buzasi, D. 2022, ApJS, 263, 41
Baliunas, S., Sokoloff, D., & Soon, W. 1996, ApJL, 457, L99
Baliunas, S. L., Donahue, R. A., Soon, W. H., et al. 1995, ApJ, 438, 269
Barnes, S. A. 2007, ApJ, 669, 1167
Baum, A. C., Wright, J. T., Luhn, J. K., & Isaacson, H. 2022, AJ, 163, 183
Boller, T., Freyberg, M. J., Trümper, J., et al. 2016, A&A, 588, A103
Boro Saikia, S., Jeffers, S. V., Morin, J., et al. 2016, A&A, 594, A29
Brewer, J. M., Fischer, D. A., Valenti, J. A., & Piskunov, N. 2016, ApJS, 225, 32
Corsaro, E., Bonanno, A., Mathur, S., et al. 2021, A&A, 652, L2
David, T. J., Angus, R., Curtis, J. L., et al. 2022, ApJ, 933, 114
Egeland, R., Soon, W., Baliunas, S., et al. 2017, ApJ, 835, 25
Finley, A. J., & Matt, S. P. 2018, ApJ, 854, 78
Finley, A. J., Matt, S. P., & See, V. 2018, ApJ, 864, 125

Folsom, C. P., Bouvier, J., Petit, P., et al. 2018, MNRAS, 474, 4956
Garraffo, C., Drake, J. J., & Cohen, O. 2015, ApJ, 813, 40
Gray, D. F., & Baliunas, S. L. 1994, ApJ, 427, 1042
Hall, O. J., Davies, G. R., van Saders, J., et al. 2021, NatAs, 5, 707
Jardine, M., Vidotto, A. A., van Ballegooijen, A., et al. 2013, MNRAS, 431, 528
Jeffers, S. V., Petit, P., Marsden, S. C., et al. 2014, A&A, 569, A79
Kochukhov, O., Makaganiuk, V., & Piskunov, N. 2010, A&A, 524, A5
Lawler, S. M., Di Francesco, J., Kennedy, G. M., et al. 2014, MNRAS, 444, 2665
Luhn, J. K., Wright, J. T., Henry, G. W., Saar, S. H., & Baum, A. C. 2022, ApJL, 936, L23
Masuda, K. 2022, ApJ, 937, 94
Mathur, S., García, R. A., Ballot, J., et al. 2014, A&A, 562, A124
McQuillan, A., Mazeh, T., & Aigrain, S. 2014, ApJS, 211, 24
Metcalfe, T. S., Egeland, R., & van Saders, J. 2016, ApJL, 826, L2
Metcalfe, T. S., Finley, A. J., Kochukhov, O., et al. 2022, ApJL, 933, L17
Metcalfe, T. S., Kochukhov, O., Ilyin, I. V., et al. 2019, ApJL, 887, L38
Metcalfe, T. S., & van Saders, J. 2017, SoPh, 292, 126
Metcalfe, T. S., van Saders, J. L., Basu, S., et al. 2021, ApJ, 921, 122
Petit, P., Dintrans, B., Solanki, S. K., et al. 2008, MNRAS, 388, 80
Réville, V., Brun, A. S., Matt, S. P., Strugarek, A., & Pinto, R. F. 2015, ApJ, 798, 116
Ryabchikova, T., Piskunov, N., Kurucz, R. L., et al. 2015, PhyS, 90, 054005
Saar, S. H., & Osten, R. A. 1997, MNRAS, 284, 803
Saar, S. H., & Testa, P. 2012, in IAU Symp. 286, Comparative Magnetic Minima: Characterizing Quiet Times in the Sun and Stars, ed. C. H. Mandrini & D. F. Webb (Cambridge: Cambridge Univ. Press), 335
Santos, A. R. G., Breton, S. N., Mathur, S., & García, R. A. 2021, ApJS, 255, 17
Santos, A. R. G., García, R. A., Mathur, S., et al. 2019, ApJS, 244, 21
See, V., Matt, S. P., Folsom, C. P., et al. 2019, ApJ, 876, 118
Stassun, K. G., Collins, K. A., & Gaudi, B. S. 2017, AJ, 153, 136
Stassun, K. G., Corsaro, E., Pepper, J. A., & Gaudi, B. S. 2018, AJ, 155, 22
Strassmeier, K. G., Ilyin, I., Järvinen, A., et al. 2015, AN, 336, 324
Tang, Y. K., & Gai, N. 2011, A&A, 526, A35
Teixeira, T. C., Kjeldsen, H., Bedding, T. R., et al. 2009, A&A, 494, 237
Torres, G., Andersen, J., & Giménez, A. 2010, A&ARv, 18, 67
Valenti, J. A., & Fischer, D. A. 2005, ApJS, 159, 141
van Saders, J. L., Ceillier, T., Metcalfe, T. S., et al. 2016, Natur, 529, 181
van Saders, J. L., & Pinsonneault, M. H. 2013, ApJ, 776, 67
van Saders, J. L., Pinsonneault, M. H., & Barbieri, M. 2019, ApJ, 872, 128
von Braun, K., & Boyajian, T. 2017, Extrasolar Planets and Their Host Stars (New York: Springer), doi:10.1007/978-3-319-61198-3
Wood, B. E. 2018, JPhCS, 1100, 012028
Wood, B. E., Müller, H.-R., Redfield, S., et al. 2021, ApJ, 915, 37
Xiang, M., Ting, Y.-S., Rix, H.-W., et al. 2019, ApJS, 245, 34